



# Corrosion protection of AA2024 by sol–gel coatings modified with MBT-loaded polyurea microcapsules

F. Maia<sup>a</sup>, K.A. Yasakau<sup>a</sup>, J. Carneiro<sup>a</sup>, S. Kallip<sup>a,\*</sup>, J. Tedim<sup>a,\*</sup>, T. Henriques<sup>b</sup>, A. Cabral<sup>b</sup>, J. Venâncio<sup>c</sup>, M.L. Zheludkevich<sup>a,d</sup>, M.G.S. Ferreira<sup>a</sup>

<sup>a</sup> CICECO – Aveiro Institute of Materials, Department of Materials and Ceramic Engineering, University of Aveiro, 3810-193 Aveiro, Portugal

<sup>b</sup> Instituto de Soldadura e Qualidade, 2740-120 Porto Salvo, Portugal

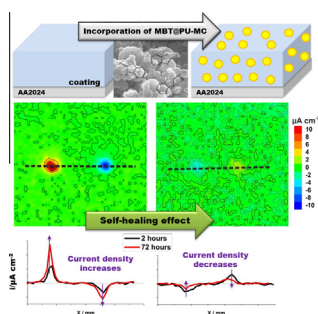
<sup>c</sup> Aerohélice Lda, Azedia, 2580-552 Alenquer, Portugal

<sup>d</sup> Institute of Materials Research, Helmholtz-Zentrum Geesthacht, Max-Planck-Str. 1, 21502 Geesthacht, Germany

## HIGHLIGHTS

- Successful encapsulation of 2-mercaptobenzothiazole in polyurea microcapsules.
- Encapsulation reduces the detrimental interaction between corrosion inhibitor and sol–gel matrix.
- Loaded microcapsules suppresses corrosion activity and improves the adhesion of sol–gel coatings to the metal substrate.
- Self-healing corrosion protective coatings for AA2024 based on modified sol–gel coating with MBT@PU-MC.

## GRAPHICAL ABSTRACT



## ARTICLE INFO

### Article history:

Received 28 April 2015

Received in revised form 20 July 2015

Accepted 31 July 2015

Available online 21 August 2015

### Keywords:

Polyurea microcapsules  
Corrosion inhibitor  
Controlled release  
Corrosion protection  
Sol–gel coating

## ABSTRACT

In this work we report the synthesis of polyurea microcapsules loaded with corrosion inhibitor 2-mercaptobenzothiazole (MBT) for corrosion protection of 2024 aluminum alloy. The microcapsules were prepared by interfacial polycondensation. The resulting capsules exhibit spherical shape, with diameter ranging between 100 nm and 2  $\mu$ m. The loading content of MBT was found to be 5 wt% and release studies showed that MBT is preferentially released under acidic and alkaline conditions and follows a Fickian diffusion model. This pH dependency seems suitable for protection of metallic alloys where corrosion processes are accompanied by local pH changes. Furthermore, the microcapsules were added to a hybrid sol–gel coating and its performance assessed by electrochemical and accelerated standard tests. The results obtained indicate that capsules loaded with MBT do not affect negatively the barrier properties of sol–gel coatings, and contribute for the enhancement of adhesion of coatings to the metallic substrate. More relevant, these additives impart active corrosion protection suppressing corrosion activity at defect sites, which opens prospects for application of polyurea microcapsules as additives for high-performance coatings.

© 2015 Elsevier B.V. All rights reserved.

## 1. Introduction

In the last decade, one of the biggest challenge in the field of corrosion has been the replacement of chromium based pre-treatments and primers by ‘green’ solutions [1]. Several

\* Corresponding author. Tel.: +351 234370255x22924.

E-mail address: [joao.tedim@ua.pt](mailto:joao.tedim@ua.pt) (J. Tedim).

approaches have been reported for aluminum alloys, especially for AA2024, because of its relevance for aeronautical industry [2].

Hybrid sol–gel coatings have been reported as promising systems for protection of aluminum alloys. They are able to establish chemical bonds with the metal surface, which renders good adhesion at the coating/metal interface [3]. Moreover, the fine tuning of properties is possible due to implicit versatility of silane chemistry and wide range of monomers available with different functionalities [4]. Nevertheless, the resulting sol–gel films can exhibit micropores and fissures, allowing the diffusion of aggressive species towards the metal surface [3], which ultimately leads to corrosion attack. Another challenging aspect associated with sol–gel coatings is the lack of active corrosion protection. To overcome this limitation different types of corrosion inhibitors have been incorporated into sol–gel coatings with the aim to confer active protection [5–9].

Generally, the direct addition of corrosion inhibitors to coating formulations is not straightforward due to compatibility issues. Some corrosion inhibitors may cause a decrease in adhesion and coating barrier properties as a result of unwanted, detrimental interactions between these active species and polymeric matrix [5,8,9]. To prevent the contact between inhibitors and coating matrix, micro and nanostructured containers have been proposed in the literature. The main role of these containers is the storage of corrosion inhibitors, reducing spontaneous leaching and providing a controlled release of inhibitor.

Several approaches for immobilization of corrosion inhibitors in reservoirs have been reported. These include anion-exchange hydroxalite loaded with decavanadate [10], organic corrosion inhibitors encapsulated in  $\beta$ -cyclodextrins [11], or SiO<sub>2</sub> nanoparticles and halloysite nanotubes loaded with azole derivatives, covered by polyelectrolyte multilayers [8,12]. More recently, other carriers for corrosion inhibitors in multifunctional coatings were suggested: TiO<sub>2</sub> nanocontainers loaded with 8-hydroxyquinoline [13], montmorillonite modified with quaternary ammonium salt [14], NaY zeolites loaded with two different inhibitors (cerium and diethyldithiocarbamate) [15] and pH-sensitive polymeric particles loaded with 8-hydroxyquinoline [16]. There are several reviews available describing the latest advances on nano and microcapsules for application in corrosion protective coatings [17,18], showing the diversity of reservoirs and the respective triggers and mechanisms of action.

Thiazole and triazole derivatives are known to be efficient corrosion inhibitors for AA2024 due to their chemisorption ability in the copper-rich intermetallic particles [8,11,12,19] and have already been encapsulated into different inorganic [20,21] and polymeric reservoirs [22].

In this work MBT was encapsulated in polyurea microcapsules. The microcapsules obtained were added to hybrid sol–gel pre-treatments for corrosion protection of AA2024. The resulting microcapsules were chemically and morphologically characterized by scanning electron microscopy (SEM), thermogravimetry (TG/DTA) and Fourier transform infrared spectroscopy (FTIR) The protective properties associated with microcapsule-containing sol–gel coatings were assessed at lab scale by electrochemical impedance spectroscopy (EIS) and the scanning vibrating electrode technique (SVET), as well as by industrial standard testing (ASTM B 117-11, NP EN ISO 2409:2012 and ISO 16276-2:2007).

## 2. Experimental section

### 2.1. Materials

Cyclohexane and *n*-butanol were acquired to Alfa Aesar and to VWR Chemicals, respectively. Span 85, diethylenetriamine (DETA) (99%), 2,4-toluene diisocyanate (TDI) (98%),

2-mercaptobenzothiazole (MBT) (97%), Poly(vinylpyrrolidone) (average mol wt 40,000) (PVP) and acetone were purchased from Sigma–Aldrich. Sodium chloride (NaCl) and buffer solutions were obtained from Riedel-de-Häen. Ethanol was supplied by Panreac. Titanium-isopropoxide (TPOT) (97%), 3-glycidoxypopyl trimethoxysilane (GPTMS) (97%) and acetylacetone were also purchased from Sigma–Aldrich. All chemicals were analytic grade and were used without further purification.

### 2.2. Synthesis of polyurea microcapsules and encapsulation of 2-mercaptobenzothiazole

The synthesis of polyurea microcapsules (PU-MC) and the encapsulation of MBT in PU-MC were performed in one single step. Two different phases were prepared, a continuous phase where the non-ionic surfactant was dissolved in water and a dispersed phase where MBT (compound to be encapsulated) was dissolved. A similar process was previously reported for the encapsulation of phenolphthalein [23], but in this case TDI was used as monomer and PVP as emulsion stabilizer. Briefly, a solution of 1 g Span 85 in 100 mL of water was prepared (continuous phase). A solution containing 0.25 g of PVP in 25 mL of water was prepared and added to the continuous phase. Then, 3 g of TDI was diluted in 20 mL of cyclohexane and, in parallel 150 mg of MBT dissolved in 10 mL of acetone. Both organic solutions were mixed (dispersed phase) and added to the continuous phase, resulting in an oil-in-water microemulsion. *n*-Butanol (1 mL) was added to the o/w microemulsion. After 15 min, 2 g of DETA were diluted in 20 mL of water and added dropwise to the microemulsion. Then, the mixture was heated until 60 °C and stirred during 3 h. The obtained precipitate was filtered, washed with pure water and dried at room temperature.

### 2.3. Characterization of polyurea microcapsules loaded with MBT

The morphology of polyurea microcapsules loaded with MBT (MBT@PU-MC) was characterized by SEM using a Hitachi S-4100 system with electron beam energy of 25 keV. Particle size distribution was determined using an image processing and analysis in Java, free software, named “ImageJ” [24]. In order to characterize the chemical and thermal properties of PU-MC, FTIR-ATR spectra were recorded with a Bruker IFS55 spectrometer equipped with a single horizontal Golden Gate ATR cell. TG/DTA was carried out in a TGA-50 Shimadzu system under air atmosphere, with a heating rate of 10 °C min<sup>-1</sup> from room temperature up to 800 °C.

### 2.4. Release studies of MBT from polyurea microcapsules

The release profiles of MBT were monitored using a UV-1600 PC Spectrophotometer from VWR. The correlation coefficient of the calibration curves obtained with 5 MBT standards was higher than 0.999.

Briefly, 100 mg of MBT@PU-MC was dispersed in 20 mL of an aqueous solution where pH was varied (4, 7 and 10) and the MBT release profiles were determined by UV-Vis spectrophotometry at specific times. 1 mL sample of the mixture was extracted with a syringe and filtered with a specific syringe filter (PTFE membrane with 0.20  $\mu$ m pore size). To determine the total amount of MBT encapsulated, 100 mg of MBT@PU-MC were dispersed in 20 mL of ethanol during 24 h to guarantee the maximum release of MBT. Ethanol was selected because MBT is very soluble in this solvent and facilitates MBT diffusion through the polymeric shell. The encapsulation efficiency was determined by the expression:

$$\%E = \frac{n_{\text{MBTExt}}}{n_{\text{MBTI}}} \times 100, \quad (1)$$

where  $n_{\text{MBT}_{\text{ext}}}$  is the amount of MBT extracted from PU-MC and  $n_{\text{MBT}_i}$  is the initial amount of MBT used in the encapsulation. TG was also used to assess the MBT loading in PU-MC.

### 2.5. Substrate preparation

Aluminum alloy 2024-T3 substrates were cleaned and etched according to a standard commercial procedure: alkaline cleaning in Metaclean T2001 at 68 °C for 15 min, alkaline etching in Turco Liquid Aluminetch N2 at 60 °C for 45 s, acid etching in Turco Liquid Smutgo NC at 30 °C for 7 min, each step followed by washing in distilled water.

### 2.6. Sol-gel preparation, application and characterization

Epoxy-functionalized SiO<sub>2</sub>/TiO<sub>2</sub> based hybrid sol-gel was prepared using a similar approach to the one previously reported, except for the use of titanium alkoxide instead of zirconium alkoxide [9]. Briefly, hybrid sols (metalorganic and organosiloxane) were prepared separately and then combined to form a hybrid solution. Titanium(IV)-isopropoxide (TPOT) was mixed with acetylacetone and stirred in a water bath at constant temperature of 22 °C during 20 min to stabilize the metalorganic precursor by acetylacetone complexant, followed by addition of 0.316 M HNO<sub>3</sub> solution (pH ~ 0.5) dropwise to start the hydrolysis process of the metalorganic compound. The solution was stirred for 60 min. In parallel, 3-glycidoxypropyltrimethoxysilane (GPTMS) was dissolved in 2-propanol in 1:1 volume proportion, followed by addition of the acidic solution with pH ~ 0.5 to promote the hydrolysis of silane and the final solution was stirred at room temperature during 60 min. After this time, both solutions were mixed and the resulting hybrid solution was stirred for 1 h at room temperature. After sol-gel synthesis, MBT (or MBT@PU-MC) were dispersed in sol-gel and stirred until obtaining a uniform dispersion.

The resulting hybrid sol-gel was applied by dip-coating onto the alloy plates for electrochemical (EIS, SVET) measurements, while samples for industrial tests were applied by spray coating. The coated plates were held in open air during 1 h to let sol-gel hydrolyze and then cured at 120 °C during 80 min in the oven. The dried thickness was measured using an “Elcometer” 456 Series Digital Coating Thickness Gauge.

Nanoindentation tests on the sol-gel coatings were performed using a CSM Micro-Hardness Tester facility and a Berkovich diamond tip was used as indenter. Hardness ( $H$ ) and Young's modulus ( $E$ ) were determined from the unloading part of the force-depth curves. Hardness was calculated as the maximum applied load over the area of contact. The hardness measurements on the sol-gel coatings were performed with a load of 1 mN corresponding to a contact depth around 300 nm.

### 2.7. Assessment of corrosion protection performance of coated AA2024-T3

EIS measurements were carried out on coated aluminum alloy 2024-T3 at room temperature in a three-electrode cell consisting of a saturated calomel reference electrode (SCE), a platinum foil counter electrode and coated AA2024-T3 plate as the working electrode in the horizontal position (an exposed area of ca. 3.3 cm<sup>2</sup>). The cell was placed in a Faraday cage to avoid the interference of external electromagnetic fields. The electrolyte was 0.5 M NaCl aqueous solution for coated plates ( $V = 10$  mL), stagnant and in equilibrium with air. The measurements were performed using a Gamry FAS2 Femtostat with a PCI4 Controller. The selected frequency range was typically from  $1 \times 10^5$  to  $1 \times 10^{-2}$  Hz, with a 10 mV RMS sinusoidal perturbation vs. open circuit potential. The impedance plots were fitted using different RC equivalent cir-

cuits, where pure capacitances were replaced by constant-phase elements (CPE). The software used for the fittings was Gamry Echem Analyst v5.61, and the  $\chi^2$  of the resulting spectra fittings varied between  $10^{-2}$  and  $10^{-4}$ .

For SVET measurements the Applicable Electronics Inc. (USA) measurement system was controlled by the ASET 2.0 software from ScienceWares Inc. (USA). The Pt-Ir vibrating microelectrode had a 10–20  $\mu\text{m}$  spherical platinum black tip. The scanning distance from surface was 100  $\mu\text{m}$ . SVET measures potential differences in solution caused by ionic fluxes arising from the sites of cathodic and anodic corrosion reactions at the surface [25]. Two artificial coating penetrating defects with diameter approximately 100  $\mu\text{m}$  and depth around 50  $\mu\text{m}$  were made by mechanical application of a stainless steel needle to all samples before immersion in 0.05 M NaCl.

Neutral salt spray (NSS) tests were performed according to Standard ASTM B 117-11 [26], where coated samples were assessed in terms of corrosion resistance in the presence of a strong electrolyte (NaCl). Adhesion corrosion tests were performed according to NP EN ISO 2409:2012 [27], where adhesion is tested in specific lattice pattern cuts made in the coatings followed by application of a pressure-sensitive tape over the lattice then removed, and according to ISO 16276-2:2007 [28], where an x-cut is made through the film to the substrate and immersed in deionized water for a defined time. All tests were performed in triplicate.

Samples used in NSS and adhesion tests were coated with a full coating system composed by the prepared sol-gel (modified with MBT@PU-MC or unmodified), followed by a waterborne primer and an epoxy based top-coat. All layers were applied by spray and the final thickness of those samples was  $50 \pm 1.5$   $\mu\text{m}$ .

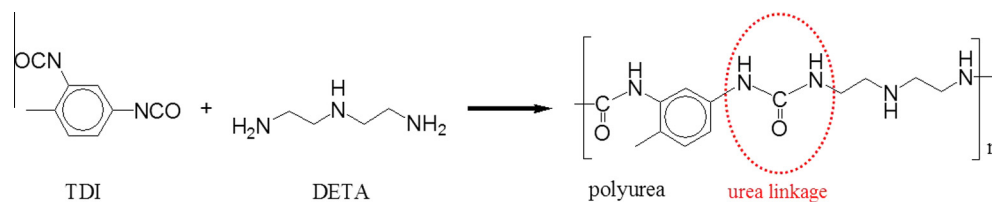
## 3. Results and discussion

### 3.1. MBT encapsulation and characterization of polyurea microcapsules loaded with MBT

Polyurea microcapsules were synthesized by interfacial polycondensation through an oil-in-water microemulsion, where the dispersed phase containing MBT was encapsulated. The polymeric shell results from the reaction of isocyanate group from TDI with amine group from DETA in the interface between the continuous phase (hydrophilic) and the dispersed phase (hydrophobic), forming a urea linkage, as represented in Scheme 1.

PU-MC prepared using this procedure have spherical and uniform morphology with a broad distribution of sizes. The encapsulation of MBT does not promote any significant modification on the microcapsules morphology when compared to empty ones, as observed in Fig. 1. The largest microcapsules show some signs of shrinkage, probably due to the high vacuum used during the SEM analysis. Both samples present signs of agglomeration. This is attributed to the drying process during sample preparation which precedes SEM analysis. To minimize this, only a small fraction of capsules was dried for characterization. The remaining material was kept in slurry form to avoid agglomeration. The mean size of obtained capsules is 277 and 219 nm for PU-MC and MBT@PU-MC, respectively. However, the standard deviation was large due to the broad size distribution and presence of microcapsules in the range of 1–2  $\mu\text{m}$ .

The obtained MBT@PU-MC present a yellow pale coloration as result of MBT encapsulation, confirming its successful immobilization. FTIR measurements allow the identification of characteristic bands associated to the urea linkage at 1641 cm<sup>-1</sup> and 1745 cm<sup>-1</sup>, corresponding to the stretching of carbonyl group and at 1551 and 3314 cm<sup>-1</sup> related to the stretching of N–H vibration from the urea linkage, directly connected to the carbonyl



**Scheme 1.** Reaction of the amine groups of DETA with isocyanate group of TDI forming the urea linkage.

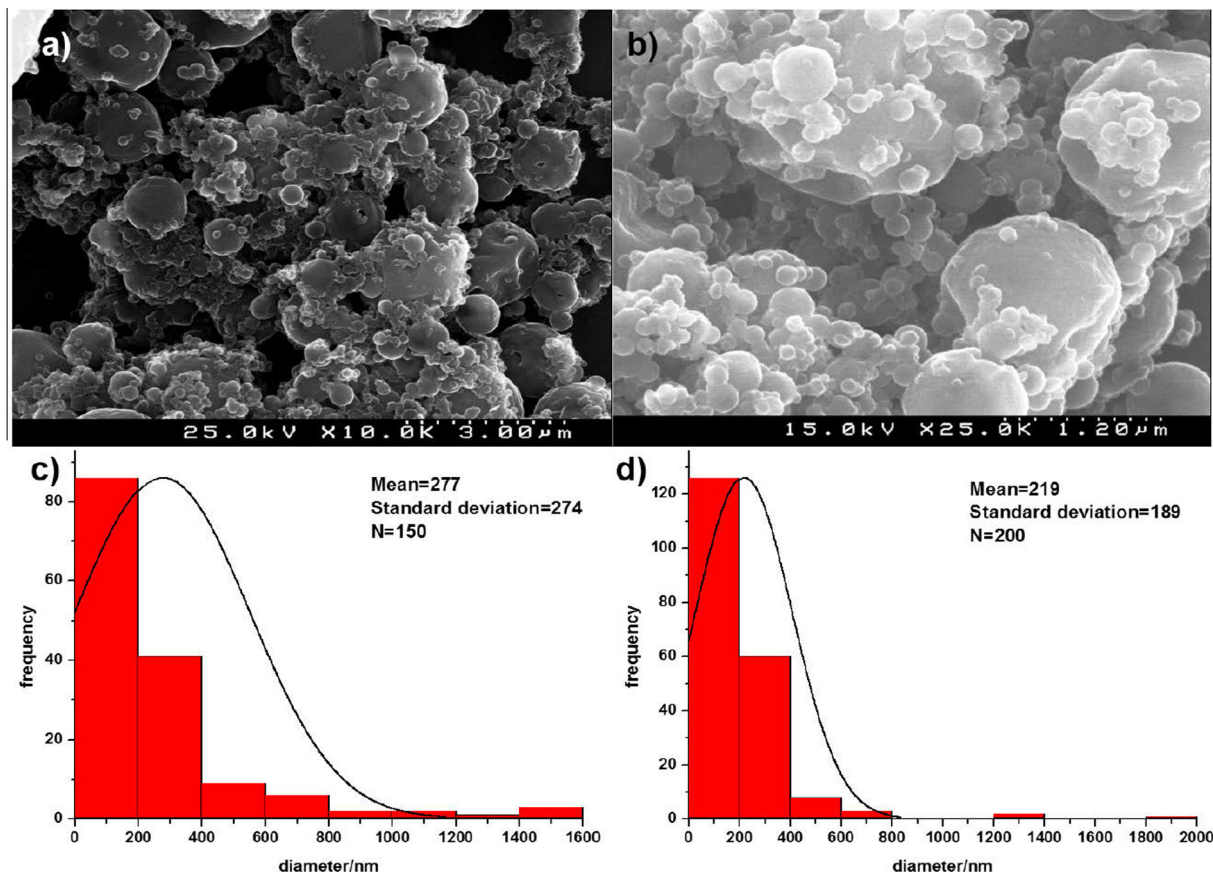


**Fig. 1.** SEM images of (a) empty PU-MC, (b) MBT@PU-MC; Size distribution histograms of (c) empty PU-MC and (d) MBT@PU-MC.

group [29], confirming the successful reaction represented in Scheme 1. Bands associated with MBT cannot be detected. This may be due to overlapping with intense bands corresponding to urea linkage.

In order to verify the thermal stability of MBT@PU-MC and to quantify the amount of MBT encapsulated in PU-MC, thermogravimetric assays were performed and the obtained data are represented in Fig. 2. Considering that both MBT and the polymeric shell (PU) are composed of organic material, they are affected by temperature in a similar way, as verified in Fig. 2. However, for MBT@PU-MC profile there is a smaller weight loss when temperature reaches 400 °C due to the presence of MBT. MBT is a well-known organic vulcanization accelerator [30] and increases the thermal resistance of rubber. In this case, this feature can be used to estimate the loading content of MBT in MBT@PU-MC. According to the difference in TG profiles between 500 and 600 °C, the value roughly estimated for MBT loading content is ~5 wt%. At temperatures higher than 600 °C all the remaining organic material is completely decomposed.

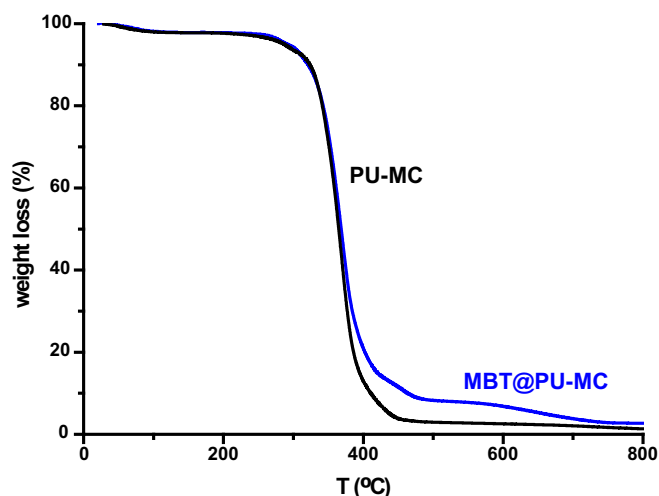


**Fig. 2.** TG profiles of empty PU-MC and MBT@PU-MC.

### 3.2. Release studies of MBT from polyurea microcapsules

The methodology used for MBT encapsulation results in an encapsulation efficiency of 32%, determined by extraction of MBT in ethanol (Eq. (1)). Ethanol was selected due to the high solubility of MBT in this solvent, and the loading content of MBT obtained in this way corresponds to 1 wt%, five times lower than the estimate from TG measurements ( $\sim 5$  wt%). Although there may be some level of uncertainty associated with the estimate of loading content by TG, one can expect that the extraction of MBT with ethanol is limited and not all MBT inside the microcapsules is quantified in this manner.

MBT@PU-MC were dispersed in aqueous solutions with different pH conditions (3, 7 and 10). These conditions were selected because pH is a corrosion relevant trigger for AA2024 since localized corrosion is accompanied with pH changes in cathodic and anodic areas. Locally, pH can reach values around 3 at anodic zones and go up to 10 in cathodic areas [31].

The release profiles of MBT are depicted in Fig. 3. The low solubility of MBT in aqueous solutions plays an important role in the extent of MBT released. Under neutral conditions the release of MBT is low, reaching only 3% of total loading content (determined by extraction with ethanol) after 48 h of immersion, while for acidic conditions this value rises up to 5% and for alkaline conditions reaches 14%. The largest release of MBT under alkaline conditions is consistent with its solubility dependence upon pH and is in agreement with release studies of MBT reported in the literature [32]. A similar pH dependence was observed for the release of phenolphthalein from PU-MC, due to the barrier effect of the capsule and the low permeability of the organic compound in the polymeric shell under these conditions [23]. More importantly, this trend (higher release in acidic and alkaline conditions) matches well the localized nature of corrosion processes in AA2024, allowing for a more effective release of inhibitor when either anodic or cathodic processes occur. On the other hand, the relative low values of MBT released can be advantageous for long-term applications.

Experimental data from MBT release profiles were fitted using established kinetic-mechanistic models. The kinetic models selected were Higuchi's square root of time (diffusion) [33] and Power Law [34] equations, presented in Table 1.  $W$  represents the percentage of MBT released at time  $t$  and  $k_1$  is the release rate constant of diffusion model. In the Power law equation,  $M_t/M_\infty$  represents the fractional drug (MBT) released into the dissolution medium and  $k_2$  is a constant incorporating structural and geometric characteristic of the material. The parameter  $n$  is a diffusion exponent that characterizes the release transport mechanism of the active. When  $n = 0.5$ , the drug diffuses through and is released from the polymeric matrix with a quasi-Fickian diffusion mechanism. For  $n > 0.5$ , anomalous, non-Fickian drug diffusion occurs, and when  $n = 1$ , a non-Fickian, Case II or zero-order release kinetics occurs [34].

The parameter which significantly affects the release of MBT from PU-MC seems to be diffusion through the polymeric walls of the microcapsules. This influence is observed by the adjustment of experimental data to the Higuchi's model, as presented in Fig. 3C and Table 1. On the other hand, Power Law model, a simple model which is typically used to characterize more complex systems also fits the experimental data with reasonable  $R^2$  values. The diffusional exponent  $n$  obtained is smaller than the theoretical value for spherical particles ( $n = 0.43$ ), probably associated with the broad distribution size diameter of MBT@PU-MC [34].

### 3.3. Coating properties and corrosion protection performance of coated AA2024-T3

MBT@PU-MC were dispersed in the prepared sol-gel and applied on etched AA2024 plates using dip-coating and spray

methods, followed by thermal curing at 120 °C. As observed before, in TG analysis (Fig. 2), MBT@PU-MC shows good thermal stability and can be used at this temperature without significant changes.

The resulting coatings show good uniformity and thickness around 2–2.5  $\mu\text{m}$  for coatings applied by dip-coating, while the ones applied by spray for industrial testing had thickness around 5  $\mu\text{m}$ .

Mechanical properties of sol-gel coating were determined by nanoindentation tests. The average values obtained for sol-gel coating was  $1.2 \pm 0.2$  GPa and  $6.4 \pm 0.7$  GPa for hardness ( $H$ ) and Young's modulus ( $E$ ), respectively. The values were calculated on the basis of five measurements. The obtained hardness value was found to be higher than the values reported in the literature, which was 0.15 GPa for GPTMS sol-gel coating [35]. The higher hardness obtained in this work is associated with the presence of titania nanoparticles (formed during the sol-gel synthesis procedure) and better reticulation of GPTMS matrix leading to a more rigid matrix. Indeed, as the inorganic content in sol-gel matrix grows both hardness and Young's modulus increase [36]. The latter was reported to be around 3–8 GPa for 25–50% of organic content in a sol-gel coating, which is consistent with our measurements.

The corrosion protection of thinner samples was assessed by EIS and SVET, while thicker samples were tested industrially under standard conditions (ASTM D1654, ISO 2409:2007 (cross-cut test) and ISO 16276-2:2007 (x-cut test)).

Fig. 4 shows Bode plots of coated AA2024 samples immersed in a 0.5 M NaCl solution after 5 days (A) and after 14 days (B). The impedance data in the high frequency range, associated with the coating response, demonstrates that when MBT is directly added to sol-gel, a significant decrease in impedance modulus ( $|Z|$ ) occurs for both times of immersion, highlighting the negative effects of the MBT directly added to sol-gel. Contrastingly, when MBT is introduced in encapsulated form that negative effect on the sol-gel coating is negligible, resulting in a similar performance as the control (undoped sol-gel) system. Therefore, encapsulation limits the negative interaction of MBT with sol-gel matrix, maintaining the barrier properties of sol-gel layer. The same behavior related to sol-gel barrier is observed even after 14 days of immersion in NaCl solution (Fig. 4B). Additionally, the coating with MBT@PU-MC exhibits the highest  $|Z|$  in the low frequency region, ascribed to a lower rate of the corrosion-related electrochemical processes on the alloy surface, thereby demonstrating the active effect of MBT in the system.

The typical Bode plot of a failed coating shows 3 time constant elements, attributed to sol-gel coating, intermediate oxide layer and corrosion activity [9]. Values of resistances and capacitances associated with those elements can be determined using equivalent circuits to fit experimental data, as represented in the scheme of Fig. 5.

The resistance associated with sol-gel coating provides valuable data on the stability of the coating upon addition of inhibiting compounds as well as on the evolution of coating barrier properties during immersion in corrosive electrolyte. On the other hand, the intermediate oxide layer is often seen on chemically cleaned alloy surface [38] and constitutes the last barrier against corrosive species. Thus, when damages occur in oxide, corrosion processes can easily initiate on the unprotected metal surface. In this context, monitoring the properties of intermediate oxide layer can unveil the improvement of corrosion protection of metal by coating with inhibitors. The evolution of sol-gel film and intermediate oxide layer resistances ( $R_{\text{coat}}$ ,  $R_{\text{ox}}$ ) during immersion in 0.5 M NaCl is depicted in Fig. 6.

The direct addition of MBT decreases the coating resistance with respect to the control system during the immersion time monitored, being more evident after 100 h of immersion until the end of the assay (Fig. 6a). On the other hand, when MBT is

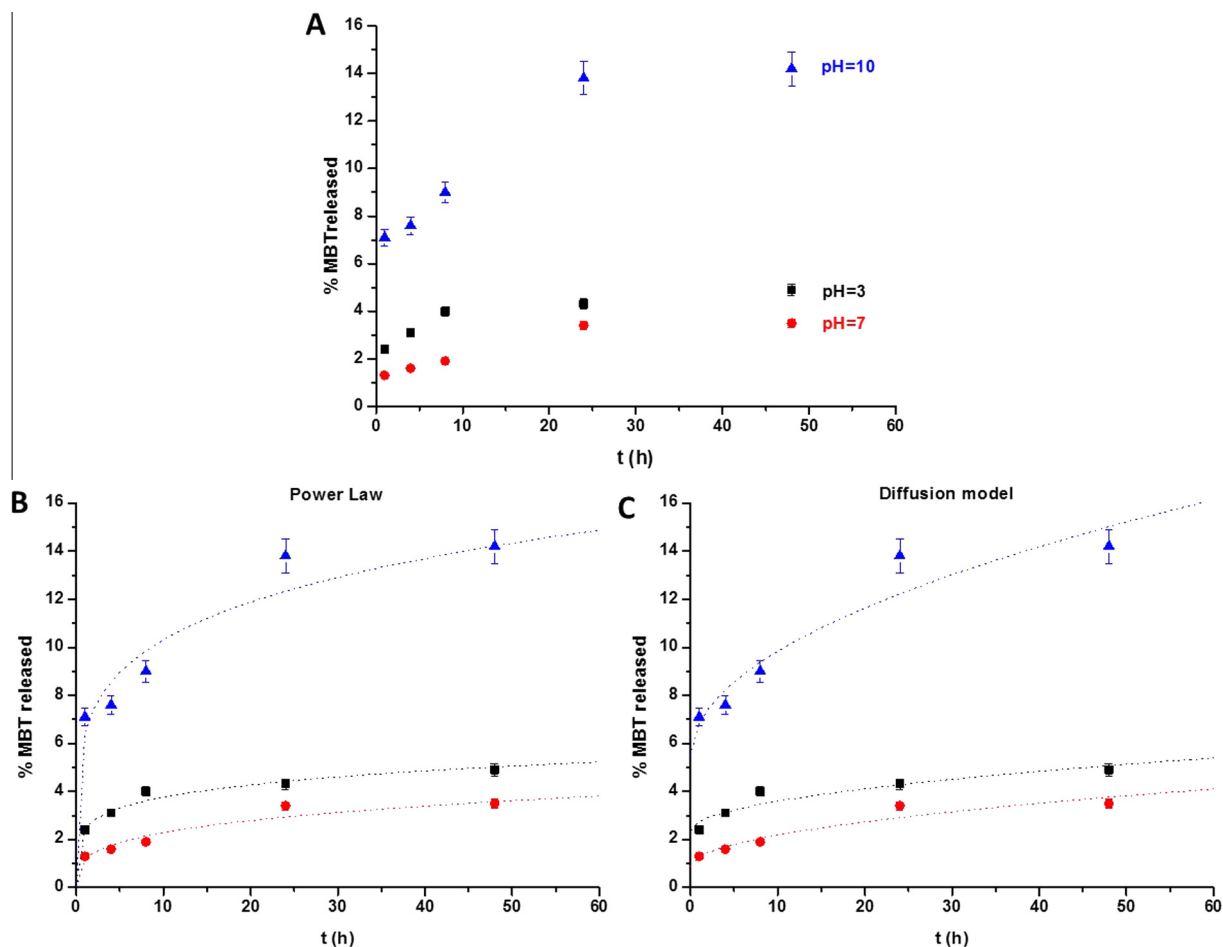


Fig. 3. (A) Release profiles of MBT from MBT@PU-MC in different pH conditions. Fittings of experimental data using different kinetic models: (B) Power Law and (C) Higuchi's square root of time (diffusion model).

Table 1  
Fitting kinetic models to MBT release experimental data at different pH's.

Kinetic models	Equation	Kinetic constants	Experimental conditions (pH)		
			3	7	10
Higuchi's square root of time	$W = k_1 t^{1/2}$	$k$	0.3926	0.4178	1.3764
		$R^2$	0.8883	0.9213	0.9196
Power law	$\frac{M_t}{M_\infty} = k_2 t^n$	$k$	0.0246	0.0119	0.0644
		$R^2$	0.9595	0.9321	0.8972
		$n$	0.1837	0.2850	0.2045

added in its encapsulated form (MBT@PU-MC) there is no decrease in the film resistance when compared to the control (undoped sol-gel) system (Fig. 6a). The same trend is observed for the intermediate oxide layer resistance. When MBT is directly added to the sol-gel,  $R_{ox}$  is similar to the control in the first measurement, but as time progress a significant decrease of approximately one order of magnitude is observed (Fig. 6b), probably due to the fast coating degradation promoted by MBT as a result of the chemical interaction between MBT and the sol-gel matrix. For MBT@PU-MC,  $R_{ox}$  values are significantly higher than control during most of the immersion time, except for the last measurement when that value is slightly lower than control (Fig. 6b). Thus, three significant conclusions can be made from EIS data analysis: the first one is the degradation of barrier properties when MBT is added directly to sol-gel, being not favorable from the point of corrosion protection; the second one is related to the preservation of sol-gel matrix

properties when MBT@PU-MC are added; and the third one is based on the improvement of corrosion protection of sol-gel modified with MBT@PU-MC observed and highlighted by higher oxide layer resistance values determined, showing signs of active corrosion protection.

The corrosion protection properties at localized defect sites were examined by SVET. All the sample coupons, with two artificially-inflicted defects made using a needle, were immersed in 0.05 M NaCl solution. Usually, the cathodic and anodic corrosion processes occur at different defects [39]. The ionic fluxes caused by these activities can be detected by SVET. In Fig. 7a the SVET maps taken after 2 h of exposure in corrosive media are presented. The reference sample shows already high current densities, while the characteristic anodic peak reaches up to  $12.1 \mu\text{A cm}^{-2}$ . The coating impregnated directly with MBT inhibitor shows only slightly lower activity ( $9.3 \mu\text{A cm}^{-2}$ ) and the sample with MBT@PU-MC stays at  $6.5 \mu\text{A cm}^{-2}$ . The visual degradation of coatings, especially at defect areas, can be seen in the optical micrographs (Fig. 7b), where the 'active spots' in the reference sample have grown more than others after 72 h of exposure in solution. The selected ionic current profiles in Fig. 7c and SVET maps at Fig. 7b demonstrate the level of corrosion activity on all samples after 72 h of immersion. The sample with MBT@PU-MC performs clearly better than the others, as the maximum anodic current density slightly decreases down to  $3.4 \mu\text{A cm}^{-2}$ , while for the reference sol-gel and coating with MBT the current densities raised up to 27.4 and  $19.2 \mu\text{A cm}^{-2}$ , respectively. These results demonstrate that the impregnation of sol-gel matrix with MBT@PU-MC gives functional

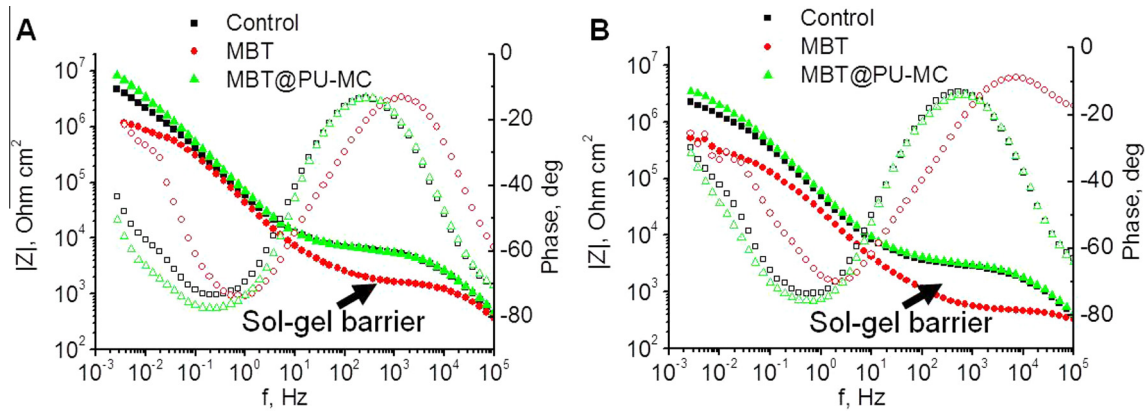


Fig. 4. Bode plots of coated AA2024 immersed in 0.5 M NaCl solution after (A) 5 days and (B) 14 days.

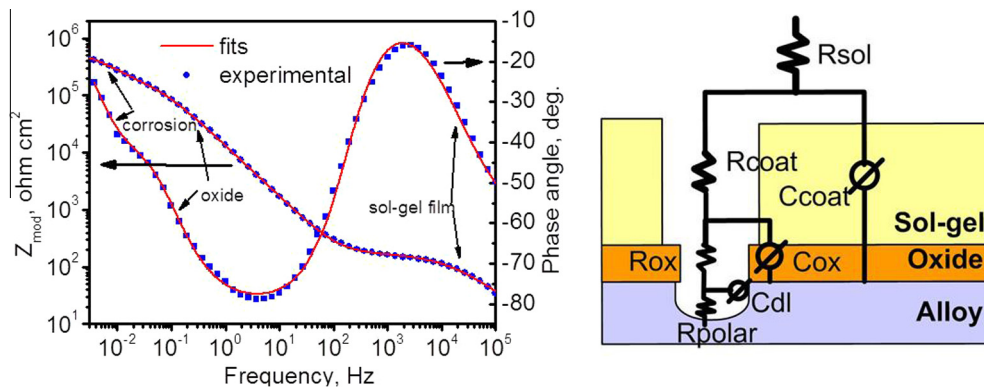


Fig. 5. Schematic representation of EIS fitted data (left) using equivalent circuits model (right). Adapted from [37].

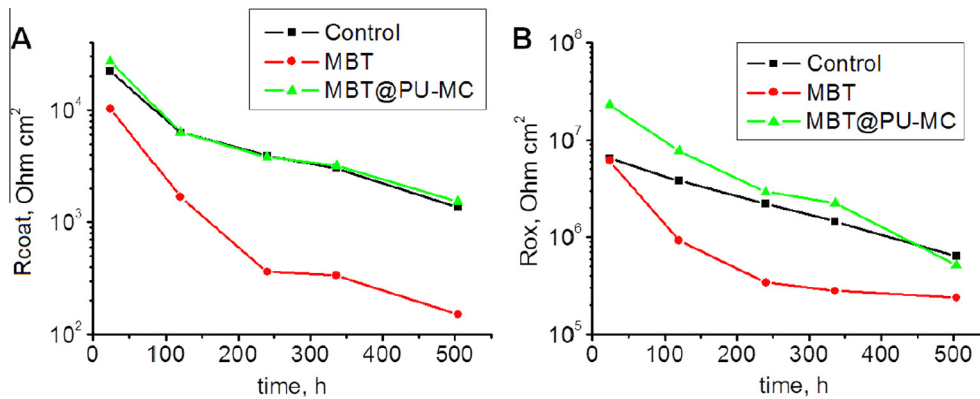


Fig. 6. Evolution of sol-gel film resistance (A) and intermediate oxide layer resistance (B) for samples with unmodified sol-gel, sol-gel with MBT and MBT@PU-MC during immersion in 0.5 M NaCl.

self-healing properties to the coating, while the direct addition of MBT corrosion inhibitor does not improve but degrades the sol-gel matrix.

Multilayer coatings ( $50 \pm 1.5 \mu\text{m}$ ), where sol-gel was applied by spray coating as pre-treatment, followed by primer and top layers, were subjected to standard tests. Coated AA2024 were placed in neutral salt spray (NSS) chamber to assess the corrosion protection in corrosive environments according to ASTM B 117-11 standard. After one week in the NSS chamber coated AA2024 samples were removed and significant differences between samples with and without MBT@PU-MC were observed, as depicted in Fig. 8. The sample coated with unmodified sol-gel presents numerous spots

of corrosion (pitting), particularly in the vicinity of the hole and on the left side of the image. Oppositely, the sample coated with sol-gel mixed with MBT@PU-MC shows several pits on the left side and no signs of pitting near the hole. This evidence suggests that MBT@PU-MC not only limits the interaction between MBT and sol-gel matrix, keeping its barrier properties, but also improves the corrosion protection of modified sol-gel on the AA2024 surface.

In addition to corrosive testing, adhesion corrosion tests were performed according to NP EN ISO 2409:2012 (cross-cut test) and ISO 16276-2:2007 (wet x-cut test), being the results shown in Figs. 9 and 10, respectively.

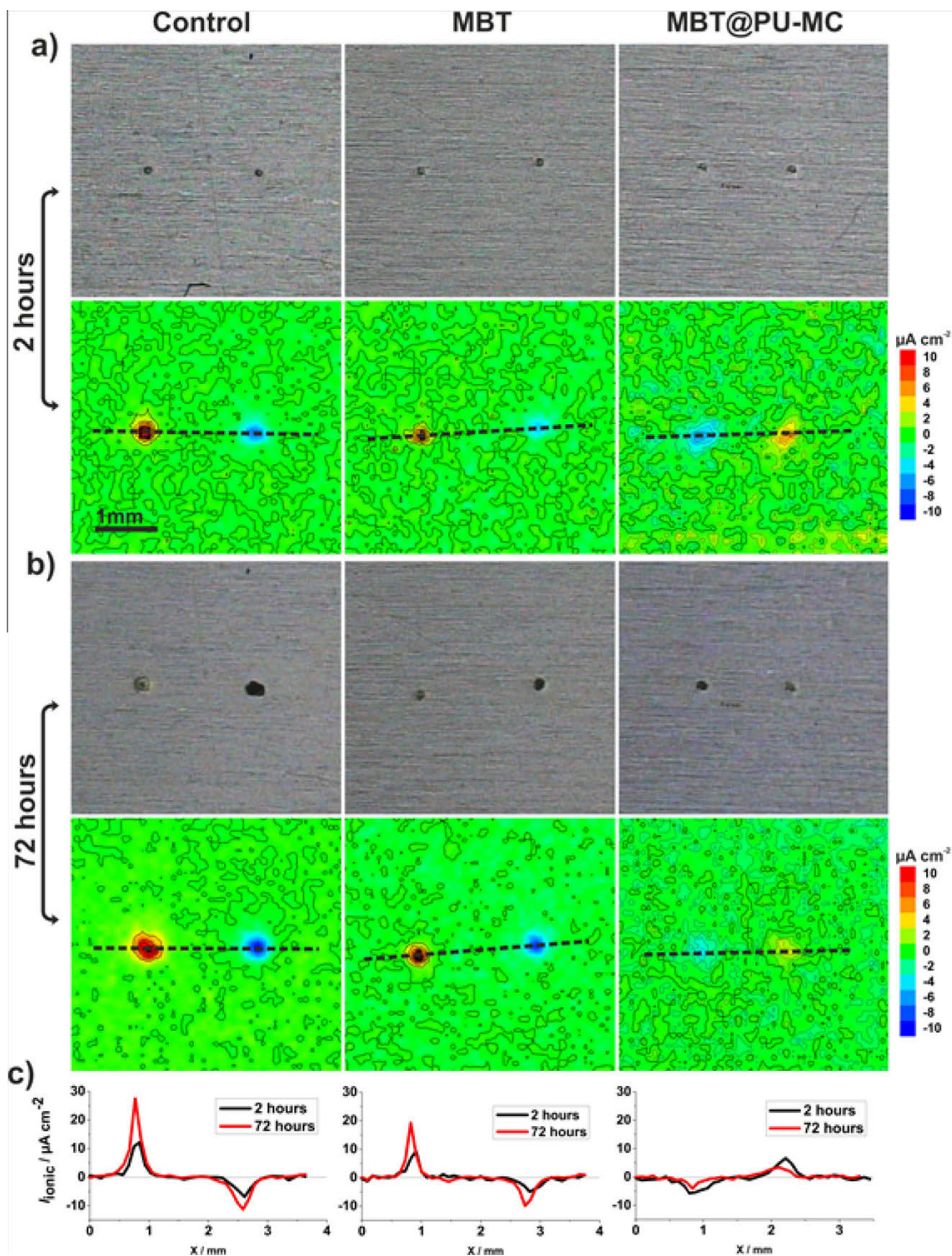


Fig. 7. Optical micrographs and SVET maps after 2 h of immersion (a) and after 72 h of immersion in 0.05 M NaCl (b) and selected ionic current profiles (c) for all samples.

Cross-cut tests show signs of separation between the coating and surface of aluminum alloy on the right angle and some delamination in a few squares for sample pre-treated with unmodified sol-gel (samples A from Fig. 9), being more evident for samples A2 and A3. According to the NP EN ISO 2409:2012 scale, sample A is classified with **3–4** (“Coating has flaked along the edges of the cuts partly or wholly in large ribbons, and/or it has flaked partly or wholly on different parts of the squares. A cross-cut area

significantly greater than 15%, but not significantly greater than 65%, is affected”). On the opposite way, samples pre-treated with sol-gel containing MBT@PU-MC (samples B from Fig. 9) show no significant signs of detachment and delamination, resulting in an improved ISO classification when MBT@PU-MC is added to the sol-gel. In this case, samples are classified with **1** (“Detachment of small flakes of the coating at the intersections of the cuts. A cross-cut area not significantly greater than 5% is affected”).



Fig. 8. Coated AA2024 with (A) unmodified sol-gel and (B) with sol-gel containing MBT@PU-MC, after 168 h in NSS.

The same trend was observed in adhesion of x-cut tests performed after immersion in deionized water and depicted in Fig. 10. The evaluation of samples was performed according to the scale used in ASTM D3359 – 09 [40]. Sample A (without sol-gel) shows trace peeling along incisions and was classified with 4A. Sample B (unmodified sol-gel + primer/top) shows trace peeling along the incision and removal at the intersection, as observed

in Fig. 10 B, being also classified with 4A. Sample C containing MBT@PU-MC in the sol-gel matrix + primer/top presents a rough surface due to the presence of some capsules aggregates, nevertheless shows no peeling or coating removal (Fig. 10 C), being classified with 5A.

According to the scale used in ASTM D3359 – 09, the adhesion of samples containing MBT@PU-MC in the sol-gel matrix shows better performance when compared with samples coated with unmodified sol-gel (sample B) and without sol-gel (sample A).

In a general way, the addition of inhibitor in encapsulated form preserves barrier properties, avoiding the negative interaction between MBT and the sol-gel matrix, observed by EIS measurements, and improves the corrosion protection as also verified by EIS and when coated samples were submitted to corrosive atmospheres in the salt spray chamber. In terms of adhesion, samples containing MBT@PU-MC also demonstrate better performance than unmodified sol-gel, for both tests realized showing less signs of detachment or delamination.

The good performance of MBT@PU-MC when incorporated in sol-gel can be attributed to the presence of two “unreacted groups” (isocyanates and amines) from the polyurea polymer used in the encapsulation of MBT and the consequent formation of microcapsules. These two groups can react with sol-gel matrix, acting not only as filler but also as crosslinking agent, improving their protective properties.

Due to the performance of MBT@PU-MC in laboratory tests and in semi-industrial scale tests, they show a high potential to be

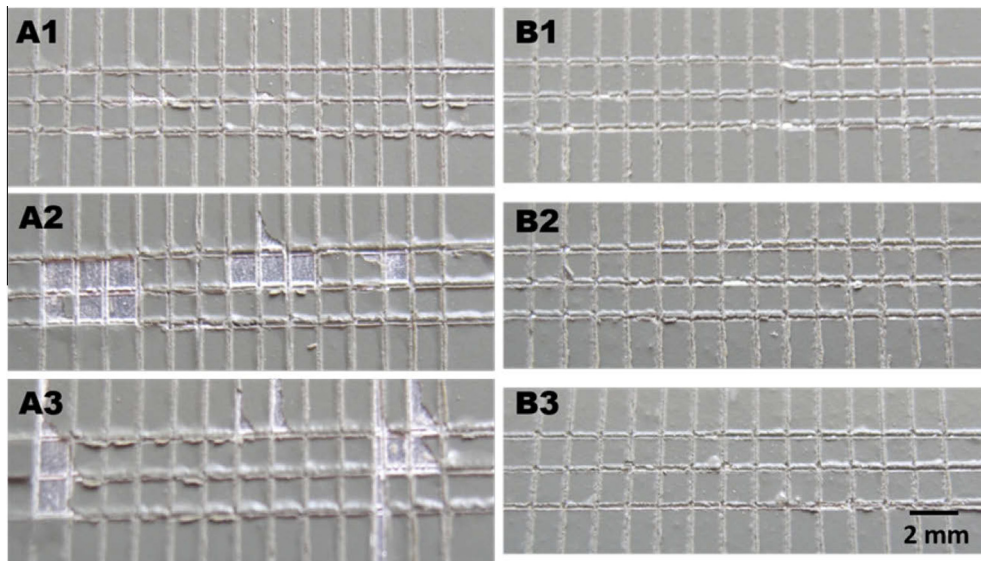


Fig. 9. Coated AA2024 with (A) unmodified sol-gel + primer/top and (B) modified sol-gel with MBT@PU-MC + primer/top, after cross-cut test.

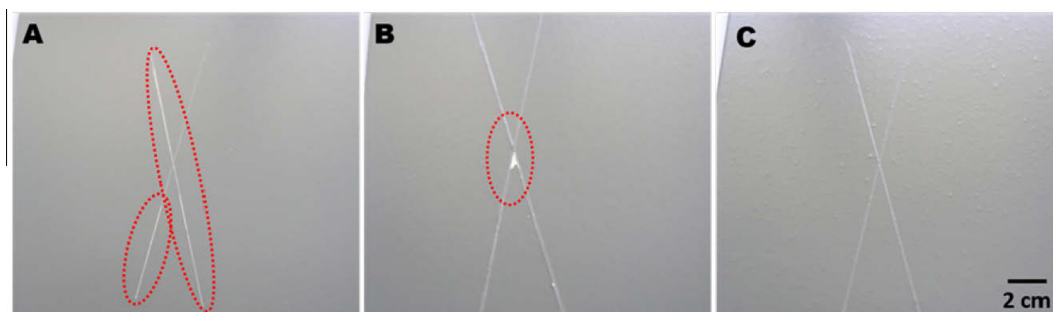


Fig. 10. Coated AA2024 with (A) primer/top, (B) unmodified sol-gel + primer/top and (C) sol-gel with MBT@PU-MC + primer/top, after wet x-cut test.

incorporated in pre-treatment or in primer corrosion protective coatings for aeronautical applications.

#### 4. Conclusions

In this work the successful synthesis and encapsulation of MBT in polyurea microcapsules is reported. As-prepared microcapsules show uniform and spherical morphology with a broad size distribution, from 100 nm up to 2  $\mu$ m. The developed microcapsules have good thermal stability up to 300 °C and have a MBT loading content around 5 wt%.

When incorporated into sol–gel matrix and applied in AA2024 pre-treatments, MBT@PU-MC corrosion protection was assessed by EIS, SVET, NSS and adhesion tests. The data obtained from different tests show the improvement of pre-treatment performance in the presence of MBT@PU-MC.

Therefore, the use of PU-MC seems an effective way of incorporating corrosion inhibitors within coating formulations, overcoming negative effects related to direct addition of inhibitors and resulting in an increase of the corrosion protective performance of the modified coating system.

#### Acknowledgements

This work was developed in the scope of the project CICECO – Aveiro Institute of Materials (Ref. FCT UID /CTM /50011/2013), financed by national funds through the FCT/MEC and when applicable co-financed by FEDER under the PT2020 Partnership Agreement and under the frame of NATAL Project Ref: 11474 Adi/QREN/FEDER.

Dr. Igor Bdikin is greatly acknowledged for the provided help with mechanical properties measurements. FM, KY, SK and JT thank FCT for PhD SFRH/BD/72663/2010, Post-Doctoral SFRH/BPD/80754/2011, and Researcher IF/00856/2013 and IF/00347/2013 grants, respectively.

#### References

- [1] R.L. Twite, G.P. Bierwagen, Review of alternatives to chromate for corrosion protection of aluminum aerospace alloys, *Prog. Org. Coat.* 33 (1998) 91–100.
- [2] J.A. DeRose, Aluminum Alloy Corrosion of Aircraft Structures: Modelling and Simulation, WIT Press, 2013.
- [3] Tammy L. Metroke, Robert L. Parkhill, Edward T. Knobbe, Passivation of metal alloys using sol–gel-derived materials – a review, *Prog. Org. Coat.* 41 (2001) 233–238.
- [4] Clément Sanchez, Beatriz Julián, Philippe Belleville, Michael Popall, Applications of hybrid organic–inorganic nanocomposites, *J. Mater. Chem.* 15 (2005) 3559–3592.
- [5] N.N. Voevodin, N.T. Grebasch, W.S. Soto, F.E. Arnold, M.S. Donley, Potentiodynamic evaluation of sol–gel coatings with inorganic inhibitors, *Surf. Coat. Technol.* 140 (2001) 24–28.
- [6] M.L. Zheludkevich, R. Serra, M.F. Montemor, K.A. Yasakau, I.M. Miranda Salvado, M.G.S. Ferreira, Nanostructured sol–gel coatings doped with cerium nitrate as pre-treatments for AA2024-T3: corrosion protection performance, *Electrochim. Acta* 51 (2005) 208–217.
- [7] A.M. Cabral, W. Trabelsi, R. Serra, M.F. Montemor, M.L. Zheludkevich, M.G.S. Ferreira, The corrosion resistance of hot dip galvanized steel and AA2024-T3 pre-treated with bis-[triethoxysilylpropyl] tetrasulfide solutions doped with Ce(NO<sub>3</sub>)<sub>3</sub>, *Corr. Sci.* 48 (2006) 3740–3758.
- [8] D.G. Shchukin, Mikhail Zheludkevich, Kiryl Yasakau, Sviatlana Lamaka, Mario G.S. Ferreira, Helmuth Möhwald, Layer-by-layer assembled nanocontainers for self-healing corrosion protection, *Adv. Mater.* 18 (2006) 1672–1678.
- [9] K.A. Yasakau, M.L. Zheludkevich, O.V. Karavai, M.G.S. Ferreira, Influence of inhibitor addition on the corrosion protection performance of sol–gel coatings on AA2024, *Prog. Org. Coat.* 63 (2008) 352–361.
- [10] G. Rudolph Buchheit, Hong Guan, Suhakar Mahajanam, Fariaty Wong, Active corrosion protection and corrosion sensing in chromate-free organic coatings, *Prog. Org. Coat.* 47 (2003) 174–182.
- [11] A.N. Khramov, N.N. Voevodin, V.N. Balbyshev, M.S. Donley, Hybrid organo-ceramic corrosion protection coatings with encapsulated organic corrosion inhibitors, *Thin Solid Films* 447–448 (2004) 549–557.
- [12] D.G. Shchukin, S.V. Lamaka, K.A. Yasakau, M.L. Zheludkevich, M.G.S. Ferreira, H. Möhwald, Active anticorrosion coatings with halloysite nanocontainers, *J. Phys. Chem. C* 112 (2008) 958–964.
- [13] E.D. Mekeridis, I.A. Kartsonakis, G.C. Kordas, Multilayer organic–inorganic coating incorporating TiO<sub>2</sub> nanocontainers loaded with inhibitors for corrosion protection of AA2024-T3, *Prog. Org. Coat.* 73 (2012) 142–148.
- [14] V. Dalmoro, J.H.Z. dos Santos, E. Armelin, C. Alemán, D.S. Azambuja, Sol–gel hybrid films based on organosilane and montmorillonite for corrosion inhibition of AA2024, *J. Colloid Interface Sci.* 426 (2014) 308–313.
- [15] E.L. Ferrer, A.P. Rollon, H.D. Mendoza, U. Lafont, S.J. Garcia, Double-doped zeolites for corrosion protection of aluminum alloys, *Micropor. Mesopor. Mater.* 188 (2014) 8–15.
- [16] D. Snihirova, S.V. Lamaka, M.M. Cardoso, J.A.D. Condeço, H.E.C.S. Ferreira, M.F. Montemor, PH-sensitive polymeric particles with increased inhibitor-loading capacity as smart additives for corrosion protective coatings for AA2024, *Electrochim. Acta* 145 (2014) 123–131.
- [17] H. Wei, Y. Wang, J. Guo, N.Z. Shen, D. Jiang, X. Zhang, X. Yan, J. Zhu, Q. Wang, L. Shao, H. Lin, S. Wei, Z. Guo, Advanced micro/nanocapsules for self-healing smart anticorrosion coatings, *J. Mater. Chem. A* 3 (2015) 469–480.
- [18] M.L. Zheludkevich, J. Tedim, M.G.S. Ferreira, “Smart” coatings for active corrosion protection based on multi-functional micro and nanocontainers, *Electrochim. Acta* 82 (2012) 314–323.
- [19] M.L. Zheludkevich, K.A. Yasakau, S.K. Poznyak, M.G.S. Ferreira, Triazole and thiazole derivatives as corrosion inhibitors for AA2024 aluminum alloy, *Corr. Sci.* 47 (2005) 3368–3383.
- [20] J. Tedim, S.K. Poznyak, A. Kuznetsova, D. Raps, T. Hack, M.L. Zheludkevich, M.G.S. Ferreira, Enhancement of active corrosion protection via combination of inhibitor-loaded nanocontainers, *ACS Appl. Mater. Interfaces* 2 (2010) 1528–1535.
- [21] F. Maia, J. Tedim, A.D. Lisenkov, A.N. Salak, M.L. Zheludkevich, M.G.S. Ferreira, Silica nanocontainers for active corrosion protection, *Nanoscale* 4 (2012) 1287–1298.
- [22] E. Koh, S.-Y. Baek, N.-K. Kim, S. Lee, J. Shin, Y.-W. Kim, Microencapsulation of the triazole derivative for self-healing anticorrosion coatings, *New J. Chem.* 38 (2014) 4409–4419.
- [23] F. Maia, J. Tedim, A.C. Bastos, M.G.S. Ferreira, M.L. Zheludkevich, Active sensing coating for early detection of corrosion processes, *RSC Adv.* 4 (2014) 17780–17786.
- [24] W. Burger, M.J. Burge, *Digital Image Processing: an Algorithmic Introduction Using Java*, Springer, London, 2008.
- [25] C. Scheffey, Two approaches to construction of vibrating probes for electrical current measurement in solution, *Rev. Sci. Instrum.* 59 (1988) 787–792.
- [26] Standard ASTM B 117–11 – “Standard Practice for Operating Salt Spray (Fog) Apparatus”.
- [27] NP EN ISO 2409:2012 – “Paints and varnishes – Cross-cut test”.
- [28] ISO 16276–2:2007 – “Corrosion protection of steel structures by protective paint systems – Assessment of, and acceptance criteria for, the adhesion/cohesion (fracture strength) of a coating – Part 2: Cross-cut testing and X-cut testing”.
- [29] M.M. Coleman, M. Sobkowiak, G.J. Pehlert, P.C. Painter, Infrared temperature studies of a simple polyurea, *Macromol. Chem. Phys.* 198 (1997) 117–136.
- [30] H.-W. Engels, H.-J. Weidenhaupt, M. Pieroth, W. Hofmann, K.-H. Menting, T. Mergenhagen, R. Schmoll, S. Uhrlandt, Rubber, 4. Chemicals and Additives. Ullmann's Encyclopedia of Industrial Chemistry, 2004.
- [31] K.A. Yasakau, M.L. Zheludkevich, S.V. Lamaka, M.G.S. Ferreira, Mechanism of corrosion inhibition of AA2024 by rare-earth compounds, *J. Phys. Chem. B* 110 (2006) 5515–5528.
- [32] J. Carneiro, J. Tedim, S.C.M. Fernandes, C.S.R. Freire, A. Gandini, M.G.S. Ferreira, M.L. Zheludkevich, Chitosan as a smart coating for controlled release of corrosion inhibitor 2-mercaptobenzothiazole, *ECS Electrochem. Lett.* 2 (2013) C19–C22.
- [33] T. Higuchi, Mechanism of sustained-action medication. Theoretical analysis of rate of release of solid drugs dispersed in solid matrices, *J. Pharm. Sci.* 52 (1963) 1145–1149.
- [34] P.L. Ritger, N.A. Peppas, A simple equation for description of solute release I. Fickian and non-Fickian release from non-swellable devices in the form of slabs, spheres, cylinders or discs, *J. Control. Release* 5 (1987) 23–36.
- [35] B.A. Latella, M. Ignat, C.J. Barbé, D.J. Cassidy, J.R. Bartlett, Adhesion behavior of organically-modified silicate coatings on stainless steel, *J. Sol-Gel. Sci. Technol.* 26 (2003) 765–770.
- [36] B.A. Latella, Indentation creep and adhesion of hybrid sol–gel coatings, *Adv. Mat. Res.* 41–42 (2008) 305–311.
- [37] M.L. Zheludkevich, D.G. Shchukin, K.A. Yasakau, H. Mohwald, M.G.S. Ferreira, Anticorrosion coatings with self-healing effect based on nanocontainers impregnated with corrosion inhibitor, *Chem. Mater.* 19 (2007) 402–411.
- [38] M.L. Zheludkevich, I.M.M. Salvado, M.G.S. Ferreira, Sol–gel coatings for corrosion protection of metals, *J. Mater. Chem.* 15 (2005) 5099–5111.
- [39] K.A. Yasakau, S. Kallip, M.L. Zheludkevich, M.G.S. Ferreira, Active corrosion protection of AA2024 by sol–gel coatings with cerium molybdate nanowires, *Electrochim. Acta* 112 (2013) 236–246.
- [40] ASTM D3359-09: Standard Test Methods for Measuring Adhesion by Tape Test.